

THREE-LEVEL NPC INVERTER FOR INTEGRATING PV AND BATTERY STORAGE USING FUZZY WITH ADVANCED CONTROL STRATEGY

B SHIVA NAGA VARAPRASAD
M-tech Student Scholar

Department of Electrical & Electronics Engineering,
LORDS Engineering College, Himayath sagar;
Ranga Reddy (Dt); Telangana, India.
Email: mercyfrank204@gmail.com

R VENKATA KRISHNA
Assoc Prof & Head,

Department of Electrical & Electronics Engineering,
LORDS Engineering College, Himayath sagar;
Ranga Reddy (Dt); Telangana, India.
Email: venkat7785@gmail.com

Abstract- A novel configuration of a three-level neutral-point-clamped (NPC) inverter that can integrate solar photovoltaic (PV) with battery storage in a grid-connected system is proposed in this paper. The strength of the proposed topology lies in a novel, it can generate the correct ac voltage under unbalanced dc voltage conditions by using three-level vectormodulation technique. The design philosophy of the proposed configuration will be presented and the theoretical framework of the proposed modulation technique. In order to control the power delivery between the solar PV, battery, and grid, which simultaneously provides maximum power point tracking (MPPT) operation for the solar PV. A new control algorithm for the proposed system is also presented. The effectiveness of the proposed methodology is investigated by the fuzzy logic simulation of several scenarios, including battery charging and discharging with different levels of solar irradiation. Here we are using the fuzzy compared to other controllers. The system performance shown in simulation results.

Index Terms—Battery storage, solar photovoltaic (PV), space vector modulation (SVM), three-level inverter Fuzzy logic control.

I. INTRODUCTION

Because of the decreasing of the fossil fuels, renewable energy sources such as photovoltaic (PV) and wind generation systems are becoming more promising alternatives to replace conventional generation units for electricity generation [1], [2]. Advanced power electronic systems are needed to utilize and develop renewable energy sources. In solar PV or wind energy applications, utilizing maximum power from the source is one of the most important functions of the power electronic systems [3]–[5]. In three-phase applications, to transfer power from the renewable energy resource to the grid two types of power electronic configurations are

commonly used: firstly single-stage another one is double-stage conversion. In the double-stage conversion for a PV system, the first stage is usually a dc/dc converter i.e chopper and the second stage is a dc/ac converter i.e inverter. The function of the dc/dc converter is to facilitate the maximum power point tracking (MPPT) of the PV array and to produce the appropriate dc voltage for the dc/ac inverter. The function of the inverter is to transfer the power to the grid in a grid-connected solar PV system or to the load in a stand-alone system to generate three-phase sinusoidal voltages or currents to transfer the power to the grid in a grid-connected solar PV system or to the load in a stand-alone system [3]–[5]. In the single-stage connection, only one converter is needed to fulfill the double-stage functions, and hence the system will have a lower cost and higher efficiency, however, a fuzzy control method will be required. The current norm of the industry for high power applications is a three-phase, single stage PV energy systems by using a voltage-source converter (VSC) for power conversion.

One of the major concerns of solar and wind energy systems is their unpredictable and fluctuating nature. Grid-connected renewable energy systems accompanied by battery energy storage can overcome this concern. This also can increase the flexibility of power system control and raise the overall availability of the system [2]. Usually, a converter is required to control the charging and discharging of the battery storage system and another converter is required for dc/ac power conversion; thus, a three phase PV system connected to battery storage will require two converters, and also the ability of controlling the battery charging and discharging. This will result in lower cost, better efficiency and increased flexibility of power flow control.

II. STRUCTURE OF A THREE LEVEL

INVERTER AND ITS CAPACITOR VOLTAGE CONSIDERATIONS

A. Three-Level Inverter

Since the introduction of three-level inverters in 1981 [6], [7], they have been widely used in several applications, such as motor drives, STATCOM, HVDC, pulse width modulation (PWM) rectifiers, active power filters (APFs), and renewable energy applications [7], [8]. Fig. 1(a) shows a typical three phase three-level neutral-point-clamped (NPC) inverter circuit topology. The converter has two capacitors in the dc side. Normally, since it has been reported that unbalance capacitor voltages can affect the ac side voltages and can produce unexpected behavior on system parameters such as even-harmonic injection and power ripple [7], [9]. Several methods have discussed by using fuzzy control for balancing these capacitor voltages in various applications

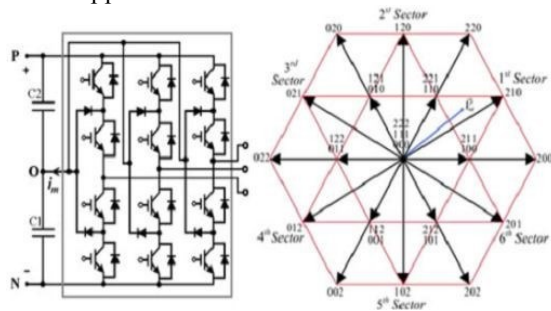


Fig. 1. Typical three-level inverter (a) structure of circuit, and (b) three-level inverter space vector diagram for balanced dc-link capacitors.

B. Balanced Capacitors

In SPWM applications, to balance the dc-link capacitors, most of the strategies are based on injecting the appropriate zero-sequence signal into the modulation signals [12], [13], [16], [18]. In SVPWM applications, to balance the dc-link capacitors a better understanding of the effects of the switching options on the capacitor voltages in the vector space has resulted in many strategies proposed.

of a three-level inverter for balanced dc-link

Using conventional SVPWM, virtual SVPWM (VSVPWM) and their combination [14], [15], [19]. These include capacitor balancing. In vector control theory, However, because of the limitation of the switches in the inverter, only a limited number of vectors (27 vectors for three-level inverter) can be generated. It is not possible to guarantee that any requested vector can be generated; as a matter of fact, To overcome such difficulties, in any space vector modulation (SVM) scheme such as SVPWM and VSVPWM, the reference vector \vec{V}_{ref} is generated by selecting the appropriate available vectors in each time frame in such a way that the average of the applied vectors must be equal to the reference vector.

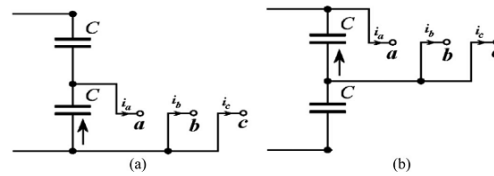


Fig. 2. Equivalent circuit and capacitors current with two different short vector. (a) Short vector—100. (b) Short vector—211

Equation (1) shows the mathematical relation between the timing of the applied vectors and the reference vector

$$T_s \vec{V}_{ref} = \sum_{i=1}^n T_i \vec{V}_i \quad (1)$$

$$T_s = \sum_{i=1}^n T_i$$

Where T_s is the time frame and preferred to be as short as possible. It can be considered as a control update period where an average vector will be mathematically generated during this time duration. T_i is the corresponding time segment for selected inverter vector V_i and n is the number of applied vectors.

Generally, the reference vector is generated by three different vector ($n=3$), and (1) can be converted to three different equation with three variables T_1 , T_2 , and T_3 to be calculated. Several vector PWM techniques presented in [6], [7], [9]–[11], and [13]–[15] apply similar technique of timing calculation. Fig. 1(b) shows the space vector diagram capacitors [6]. It is made up of 27 switching states, from which 19 different voltage vectors can be

selected. The number associated with each vector in Fig. 1(b) represents the switching state of the inverter phases respectively. The voltage vectors can be categorized into five groups, in relation to their amplitudes and their effects on different capacitor voltages from the view of the inverter ac side. For generating \vec{V}_{ref} , when one of these selections (\vec{V}_i), is a short vector, then there are two choices that can be made which can produce exactly the same effect on the ac side of the inverter in the three wire connection (if voltages are balanced).

For example, the short vector “211” will have the same effect as “100” on the ac side of the inverter. However, this choice will have different effect on the dc side, as it will cause a different dc capacitor to be chosen for the transfer of power from or to the ac side, and a different capacitor will be charged or discharged depending on the switching states and the direction of the ac side current. For example, Fig. 2 shows the connection of the capacitors when “100” or “211” is selected, demonstrating how different capacitors are involved in the transfer of power. Capacitor balancing in most reported three-level NPC inverter applications is achieved by the proper selection of the short vectors. In order to produce the ac-side waveform, the vector diagram of Fig. 1(b) is used, where the dc capacitor voltages are assumed to be balanced. Fig. 1(b) can then be used to determine the appropriate vectors to be selected and to calculate their corresponding timing (T_i) for implementing the required reference vector based on the expression given in (1). Although the control system is trying to ensure balanced capacitor voltages, should any unbalance occur during a transient or an unexpected operation, the above method will produce an inaccurate ac-side waveform which can be different from the actual requested vector by the control system.

This can result in the production of even-harmonics, unbalanced current and unpredicted dynamic behavior. However, in some applications, the requirement of having balanced capacitor voltages may be too restrictive. It is possible to work with either balanced or unbalanced capacitor voltages. The method proposed in this paper is based on the freedom of having balance or unbalanced capacitor voltages. In such applications, it is important to be able to generate an accurate reference vector based on (1), irrespective of whether the

capacitor voltages are balanced or not, to achieve the desired objectives of the system

C. Unbalanced Capacitor Voltages

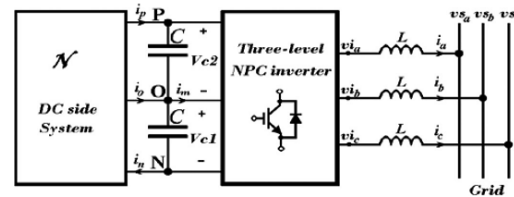


Fig. 3. General diagram of a grid connected three-wire three-level inverter

Fig. 3 shows a general structure of a grid-connected three level inverter showing the dc and ac sides of the inverter. The dc-side system, shown as “N” can be made up of many circuit configurations, For instance, depending on the application of the inverter. The dc-side system can be a solar PV, a wind generator with a rectifying circuit, a battery storage system or a combination of these systems where the dc voltage across each capacitor can be different or equal. One of the main ideas of this paper is to have an overall view of the switching effects on a three-wire connection of a three-level NPC inverter with a combination of these systems on the dc side as well as to improve the efficiency and reduce the losses by using fuzzy logic control. . Mathematically, in a three-wire connection of a two-level inverter, the $dq0$ field, V_d , V_q , and V_0 of the inverter in vector control can be considered as having two degrees of freedom in the control system; because the zero sequence voltage, v_0 will have no effect on the system behavior in both the dc and the ac side of the inverter. However, in the three-level three-wire application illustrated in Fig. 3, with fixed V_d and V_q although V_0 will have no effect on the ac-side behavior, it can be useful to take advantage of V_0 to provide a new degree of freedom to control the sharing of the capacitor voltages in the dc bus of the inverter. By doing this, it is now possible to operate and control the

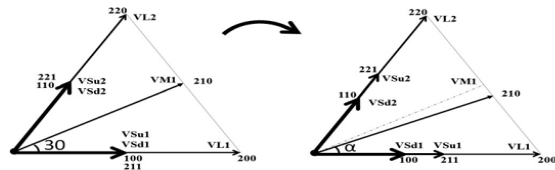


Fig. 4. Vector diagram in the first sector of Fig. 1(b) showing the change of the vectors using balanced dc and unbalanced dc assuming $V_{C1} < V_{C2}$.

D. Effect of Unbalanced Capacitor Voltages on the Vector Diagram

In the vector diagram shown in Fig. 1(b), to have different magnitudes and angles compared to the case capacitor voltage unbalance causes the short and medium vectors when the capacitor voltages are balanced. Fig. 4 shows the differences between two cases as highlighted in the first sector of the sextant in Fig. 1(b) for $V_{C1} < V_{C2}$. Vector related to the switching state \vec{V}_I can be calculated as follows [20]:

$$\vec{V}_I = \frac{2}{3} (\vec{V}_{aN} + \vec{V}_{bN} + \vec{V}_{cN}) \quad (2)$$

Where $\vec{a} = e^{j\omega t}$ and V_{aN}, V_{bN} and V_{cN} are the voltage values of each phase with reference to "N" in Fig. 1(a). Assuming that the length of the long vectors ($(2/3)V_{dc}$) is 1 unit and the voltage of capacitor C1, $V_{C1} = hV_{dc}$, for $0 \leq h \leq 1$, then the vectors in the first sector can be calculated using (2) and the results are given in (3)–(9)

$$\vec{V}_{sd1} = h \quad (3)$$

$$\vec{V}_{su1} = 1 - h \quad (4)$$

$$\vec{V}_{i2} = \frac{1}{2} + \frac{\sqrt{3}}{2} j \quad (6)$$

$$\vec{V}_{su2} = h \left(\frac{1}{2} + \frac{\sqrt{3}}{2} j \right) \quad (7)$$

$$\vec{V}_{su2} = (1-h) \left(\frac{1}{2} + \frac{\sqrt{3}}{2} j \right) \quad (8)$$

$$\vec{V}_{m1} = (1-h) + h \frac{\sqrt{3}}{2} \quad (9)$$

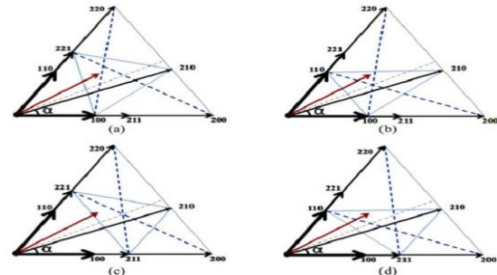


Fig. 5. Different possible vector selection ideas. The vectors in the other sectors can be calculated similarly. Equations (3)–(9) show that the magnitudes and depending on the value of the

capacitor voltages the angles of the vectors can change. For example, when $h=0.5$, then the two capacitor voltages are the same and the two short vectors are the same, $\vec{V}_{s11} = \vec{V}_{su1}$.

However, the vectors will have different magnitudes when the two capacitor voltages are different. Since the short vectors are now different in magnitude, the choice of these short vectors will now have a different effect on both the dc and ac side. Traditionally, each pair of short vectors is considered to be redundant, as the selection of any of the short vectors at any instance will have the same effect on the ac side. However, when the two capacitor voltages are different, the short vectors cannot be considered to be redundant anymore.

E. Selecting Vectors Under Unbalanced DC Voltage Condition and Their Effects on the AC Side of Inverter

To generate a reference vector based on (1), different combinations can be implemented. Fig. (5) shows different possible vector selections to generate a reference vector (\vec{V}^*) in the first sector based on the selections of different short vectors. For example, to generate (\vec{V}^*) based on fig. 5(a), one of the following combinations can be selected with proper timing based on (1). The combinations are (221-210-100),

(221-220-100), (221-200-100), (221-200-Zero), (220-200-Zero), where “zero” can be “000” or “111” or “222”. This demonstrates that there is flexibility in choosing the correct vector selections. Although all of these selections with suitable timing can generate the same reference vector, they have different impacts on the dc side and ac side of the inverter in their instantaneous behavior.

To investigate the ac-side behavior, the accuracy of the generated voltage must be examined. As far as the ac side is concerned, ideally the requested voltage $\vec{V}^*(t)$ should be exactly and simultaneously generated in the three phases of the inverter to have the correct instantaneous current in the ac side of the system. However, because of the limitation of the inverter to generate the exact value of the requested voltage in each phase, in the short time T_s , only the average value of the requested vector \vec{V}^* for the specified time window of T_s can be produced.

$$\vec{e}(t) = \vec{V}^*(t) - \vec{V}_{ap1}(t) \quad (10)$$

$$E(t) \triangleq \int_0^t \vec{e}(t) dt; \quad 0 \leq t \leq T_s \quad (11)$$

where $V_{ap1}(t)$ is the applied vector at the time “t”. This error can result in harmonic current across the impedance connected between the inverter and the grid. If this impedance is an inductor then the ripple in the inductors current I_{rL} can be expressed as

$$\vec{I}_{rL} = 1/L \int_0^t \vec{e}(t) dt \quad (12)$$

Where $\vec{e}(t)$ is defined as

based on (1) and (11), $E(T_s) = 0$ or the sum of errors during the period T_s is zero; but to reduce the error $\vec{e}(t) \triangleq \frac{dE(t)}{dt}$ (13)

To derive (13), it is assumed that the requested vector $\vec{V}^*(t)$ will generate sinusoidal current in the inductor, which is normally acceptable in the continuous time behavior of the system. Based on (11) and (12), the

absolute value of error $E(t)$ is directly related to the

magnitude of high frequency ripples, it is important to minimize the error at each time instant. To achieve this, the three nearest vectors (TNV) are usually used. For example, in Fig. 5(a), to generate the requested vector \vec{V}^* , in the TNV method, the group (221, 210, 100, or 211) appears to be the best three nearest vectors to be chosen. Also, to reduce $E(t)$, a smart timing algorithm for each vector in the TNV method has been proposed, such as dividing the time to apply each vector into two or more shorter times. However, this will have the effect of increasing switching losses. Dividing by two is common, acceptable solution. Moreover, reducing T_s will reduce the error $E(t)$ while improving the accuracy of the requested vector generated by the control system. According to the basic rule of digital control, accuracy of the requested vector calculation can be improved by reduction of the sampling time and the vector calculation time.

F. Selecting Vectors Under Unbalanced DC Voltage Conditions and Their Effects on DC Side of the Inverter

As far as the dc side is concerned, different vectors have different effects on the capacitor voltages which depend on the sum of the incoming currents from the dc side and the inverter side. Fig. 3 shows i_p , i_o , and i_n as dc-side system currents which are dependent on the dc-side system circuit topology and capacitor voltages. The currents coming from the inverter are related to the inverter switching and the ac side of inverter currents which can be directly affected by the implemented vectors in the inverter. Selecting different vectors will transfer ac-side currents and power differently to the capacitors as discussed in Section II-B. The instantaneous power transmitted to the dc side of the inverter from the ac side can be calculated as follows:

$$p(t) = r_{1a} \cdot i_a + r_{1b} \cdot i_b + r_{1c} \cdot i_c \quad (14)$$

Where v_{1a} , v_{1b} , and v_{1c} are the ac-side inverter instantaneous voltages with reference to the “N” point, and i_a , i_b , i_c are inverter currents. For example, in the first sector of the vector diagram shown in Fig. 4, $p(t)$ for the short vectors can be expressed by the following equations:

$$\begin{cases} P_{211}(t) = (1-h)V_{dc} * i_a \\ P_t = hV_{dc} * (-i_a) \end{cases} \quad (15)$$

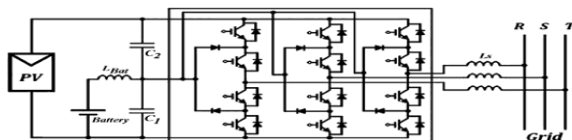
$$\begin{cases} P_{220}(t) = (1 - h)V_{dc} * (-i_c) \\ P_{110}(t) = hV_{dc} * i_c \end{cases} \quad (16)$$

Ignoring the dc-side system behavior, selecting the upper short vectors, “211” and “221,” will affect the upper capacitor voltage, and selecting the lower short vectors, “100” and “110,” will affect the lower capacitor voltage. For example, when $i_a > 0$, if vector “211” is selected, it will charge the upper capacitor without any effect on the lower capacitor voltage and if vector 100 is selected, it will discharge the lower capacitor without having any effect on the upper capacitor voltage. By using (15) and (16), the rate of charging and discharging and their dependency on h and V_{dc} values and inverter currents can also be observed. However, for accurate investigations, the dc side system behavior needs to be considered in the control of charging and discharging rates of the capacitor voltages.

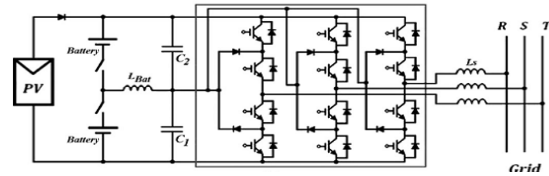
III. PROPOSED TOPOLOGY TO INTEGRATE SOLAR PV AND BATTERY STORAGE AND ITS ASSOCIATED CONTROL

A. Proposed Topology to Integrate Solar PV and Battery Storage

Using an Improved Unbalanced DC Functionality of a Three-Level Inverter Based on the discussions in Sections I and II, two new configurations of a three-level inverter to integrate battery storage and solar PV shown in Fig. 6 are proposed, where no extra converter is required to connect the battery storage to the grid connected PV system. These can reduce the cost and improve the overall efficiency of the whole system particularly for medium and high power applications



(a)



(b) Fig. 6. Proposed configurations for integrating solar PV and battery storage (a) basic configuration; (b) improved configuration.

Fig. 6(a) shows the diagram of the basic configuration. In the proposed system, to the grid power can be transferred from the renewable energy source while allowing charging and discharging of the battery storage systems as requested by the control system. To achieve the MPPT condition the proposed system will be able to control the sum of the capacitor voltages ($V_{C1} + V_{C2} = V_{dc}$) and at the same time will be able to control independently the lower capacitor voltage (V_{C1}) that can be used to control the charging and discharging of the battery storage system. Further, the output of the inverter can still have the correct voltage waveform with low total harmonic distortion (THD) current in the ac side even under unbalanced capacitor voltages in the dc side of the inverter. Although this configuration can operate under most conditions, however when the solar PV does not produce any power, the system cannot work properly with just one battery. Fig. 6(b) shows the improved configuration where two batteries are now connected across two capacitors through two relays. When one of the relays is closed and the other relay is open, the configuration in Fig. 6(b) is similar to that in Fig. 6(a) which can charge or discharge the battery storage while the renewable energy source can generate power. However, when the renewable energy is unavailable, both relays can be closed allowing the dc bus to transfer or absorb active and reactive power to or from the grid. It should be noted that these relays are selected to be ON or OFF as required; there is no PWM control requirement.

This also provides flexibility in managing which of the two batteries is to be charged when power is available from the renewable energy source or from the grid. The relay connected to this battery can be opened when one of the batteries is fully charged, while closing the relay on the other battery to charge. Special consideration needs to be made to ensure that current through the inductor L_{batt} must be

zero prior to opening any of these relays to avoid disrupting the inductor current and also to avoid damaging the relay.

B. Control Topology:

In Fig. 6(b), three different relay configurations can be obtained: 1) when the top relay is closed; 2) when the bottom relay is closed; and 3) when both relays are closed.

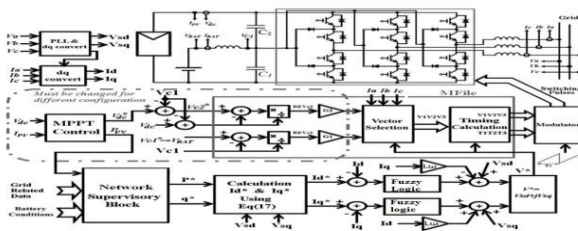


Fig. 7. Control system diagram to integrate PV and battery storage.

Fig. 7 shows the block diagram of the control system for configuration 1). In Fig. 7, the requested active and reactive power generation by the inverter to be transferred to the grid will be determined by the network supervisory block. based on the available PV generation, this will be achieved the grid data, and the current battery variables. The MPPT block determines the requested dc voltage across the PV to achieve the MPPT condition. By using another control loop this voltage can be determined, with slower dynamics, using the measurement of the available PV power.]. Based on the requested active (p*) and reactive power (q*), and the grid voltage in the dq-axis, v_{sd} and v_{sq}, the requested inverter current in the dq-axis, i_d and i_q can be obtained using voltages, and V_{C1} and V_{C2} are the actual capacitor voltages for capacitor C₁ and C₂, respectively. which capacitor is to be charged or discharged the selection of the short vectors will be determined. which short vector must be selected to determine, the relative errors of capacitor voltages and their effectiveness on

$$i_d^* = \frac{p}{r_{sd}^2 + r_{sq}^2} r_{sd} - \frac{q}{r_{sd}^2 + r_{sq}^2} r_{sq}, \quad i_q^* = \frac{q}{r_{sd}^2 + r_{sq}^2} r_{sd} + \frac{p}{r_{sd}^2 + r_{sq}^2} r_{sq} \quad (17)$$

By using a fuzzy logic control voltage vector can be calculated. The proposed control system is shown in

Fig. 7. In the proposed system, to transfer a specified amount of power to the grid, the battery will be charged using surplus energy from the PV or when the available energy cannot support the requested power will be discharged to support the PV. After evaluating the requested reference voltage vector, the appropriate sector in the vector diagram can be determined. which short vectors are to be selected, the relative errors of capacitor voltages given in (18) and (19) are used

$$e_{vc1} = \frac{V_{C1}^* - V_{C1}}{V_{C1}} \quad (18)$$

$$e_{vc2} = \frac{V_{C2}^* - V_{C2}}{V_{C2}} \quad (19)$$

Where V_{C1}^{*} and V_{C2}^{*} are the desired capacitor the control system behavior are important. A decision function “F”, as given in (20), can be defined based on this idea

$$F = G_1 e_{vc1} - G_2 e_{vc2} \quad (20)$$

where G₁ and G₂ are the gains associated with each of the relative errors of the capacitor voltages. To determine which relative error of the capacitor voltages G₁ and G₂ are used is more important and consequently it allows better control of the chosen capacitor voltage. For example, for an application that requires the balancing of the capacitor voltages as in traditional three-level inverters, G₁ and G₂ must have the same value with equal reference voltage values, but in the proposed application where the capacitor voltages can be unbalanced, G₁ and G₂ are different and their values are completely dependent on their definitions of desired capacitor voltages

In each time step, to determine which short vectors are to be chosen the sign of F is used. When F is positive, the short vectors need to be selected that can charge C₁ or discharge C₂ in that particular time step by applying (14) and using similar reasoning to

(15) and (16). Similarly, the short vectors need to be selected that can charge C₂ or discharge C₁ in that particular time step when F is negative. Based on the control system diagram given in Fig. 7, on the ac side, the requested active power p*, and reactive

power q^* , will be generated by the inverter by implementing the requested voltage vector and applying the proper timing of the applied vectors. Further, on the dc side, MPPT control can be achieved by strict control of V_{C2} ($G2 \gg G1$) with reference value of $(V_{dc}^* - V_{C1})$ and more flexible control of V_{C1} with reference value of the battery voltage, V_{BAT} .

By using the decision function (F) with the given reference values, to implement the requested vector can be determined. The proper short vectors to be applied. With MPPT control, the PV arrays can transfer the maximum available power (PPV), and with generating the requested vector in the ac side, the requested power P^* is transferred to the grid. Then, control system will automatically control V_{C1} to transfer excess power ($P_{PV} - P^*$) to the battery storage or absorb the power deficit ($P^* - P_{PV}$) from the battery storage. 1) The same control system is applicable for configuration 2) by changing the generated reference voltages for the capacitors. Configuration 3) It represents two storage systems connected to grid without any PV contribution, such as at night when the PV is not producing any output power.

A. First Theoretical Scenario

In the first scenario, it is assumed that the solar irradiation will produce $I_{sc} = 5.61A$ in the PV module according to (21). The MPPT control block, shown in Fig. 7, determines the requested PV module voltage V_{dc}^* , which is 117.3 V to achieve the maximum power from the PV system that can generate 558 W of electrical power. The requested active power to be transmitted to the grid is initially set at 662 W and is changed to 445 W at time $t = 40$ ms and the reactive power changes from zero to 250 VAR at $t = 10$ ms.

B. Second Theoretical Scenario

In the second scenario, it is assumed that the solar irradiation will change such that the PV module will produce $I_{sc} = 4.8, 4,$ and $5.61A$. The MPPT control block determines that V_{dc}^* needs to be 115.6, 114.1, and 117.3 V to achieve the maximum power from the PV units which can generate 485, 404, and 558 W respectively.

C. Practically Oriented Simulation

In the third simulation, the requested active

power to be transmitted to the grid is initially set at 295 W and, at time $t = 40$ ms, the requested active power starts to reduce as a slope controlled change and is finally stays constant at 165 W at $t = 90$ ms. It is assumed that the solar irradiation will produce $I_{sc} = 2.89$ A in the PV module according to (21). The requested PV module voltage V_{dc}^* to achieve MPPT condition will be 112.8 V to generate 305 W of electrical power

IV. FUZZY LOGIC CONTROLLER

In FLC, basic control action is determined by a set of linguistic rules. These rules are determined by the system. Since the numerical variables are converted into linguistic variables, mathematical modeling of the system is not required in FC.

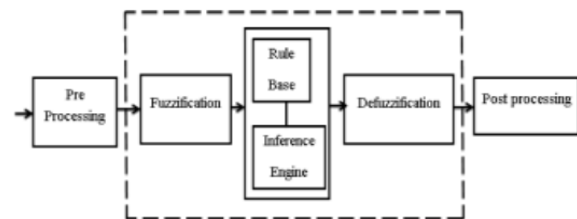


Fig.8. Fuzzy logic controller

The FLC comprises of three parts: fuzzification, interference engine and defuzzification. The FC is characterized as i. seven fuzzy sets for each input and output. ii. Triangular membership functions for simplicity. iii. Fuzzification using continuous universe of discourse. iv. Implication using Mamdani's, 'min' operator. v. Defuzzification using the height method.

TABLE I: Fuzzy Rules

Change in error	Error						
	NB	NM	NS	Z	PS	PM	PB
NB	PB	PB	PB	PM	PM	PS	Z
NM	PB	PB	PM	PM	PS	Z	Z
NS	PB	PM	PS	PS	Z	NM	NB
Z	PB	PM	PS	Z	NS	NM	NB
PS	PM	PS	Z	NS	NM	NB	NB
PM	PS	Z	NS	NM	NM	NB	NB
PB	Z	NS	NM	NM	NB	NB	NB

Fuzzification: Membership function values are assigned to the linguistic variables, using seven fuzzy subsets: NB (Negative Big), NM (Negative Medium),

NS (Negative Small), ZE (Zero), PS (Positive Small), PM (Positive Medium), and PB (Positive Big). The Partition of fuzzy subsets and the shape of membership $CE(k)$ $E(k)$ function adapt the shape up to appropriate system. The value of input error and change in error are normalized by an input scaling factor.

In this system the input scaling factor has been designed such that input values are between -1 and +1. The triangular shape of the membership function of this arrangement presumes that for any particular $E(k)$ input there is only one dominant fuzzy subset. The input error for the FLC is given as

$$E(k) = \frac{P_{ph}(k) - P_{ph}(k-1)}{V_{ph}(k) - V_{ph}(k-1)} \quad (21)$$

$$CE(k) = E(k) - E(k-1) \quad (22)$$

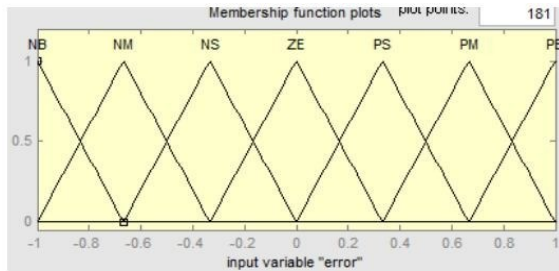


Fig.9. Membership functions

Inference Method: Several composition methods such as Max–Min and Max-Dot have been proposed in the literature. In this paper Min method is used. The output membership function of each rule is given by the minimum operator and maximum operator. Table 1 shows rule base of the FLC.

Defuzzification: As a plant usually requires a non-fuzzy value of control, a defuzzification stage is needed. To compute the output of the FLC, “height” method is used and the FLC output modifies the control output. Further, the output of FLC controls the switch in the inverter. In UPQC, the active power, reactive power, terminal voltage of the line and capacitor voltage are required to be maintained. In order to control these parameters, they are sensed and compared with the reference values. To achieve this, the membership functions of FC are: error, change in error and output

The set of FC rules are derived from

Where α is self-adjustable factor which can regulate the whole operation. E is the error of the system, C is the change in error and u is the control variable. A large value of error E indicates that given system is not in the balanced state. If the system is unbalanced, the controller should enlarge its control variables to balance the system as early as possible. On the other hand, small value of the error E indicates that the system is near to balanced state.

IV. SIMULATION AND VALIDATION OF THE PROPOSED TOPOLOGY AND CONTROL SYSTEM

Simulations have been carried out using MATLAB/Simulink to verify the effectiveness of the proposed topology and control system. To connect the inverter to the grid an LCL filter is used.

$$u = -[\alpha E + (1-\alpha) * C] \quad (23)$$

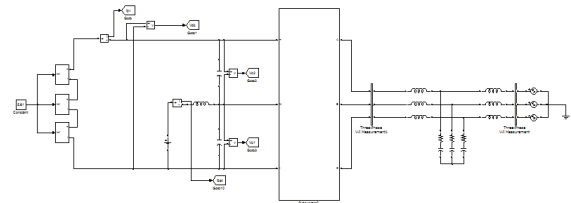


Fig. 10. Simulated model of the proposed system

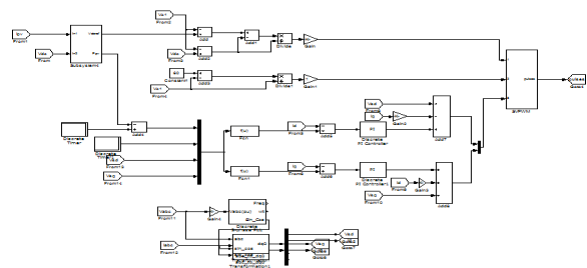


Fig. 11. Control model of the proposed system in simulation

TABLE II

PARAMETERS OF THE SIMULATED SYSTEM

V_{BAT}	V_s (line)	L_{BAT}	C_1, C_2	L_f	L_g
60 V	50 V	5 mH	1000 uF	500 uH	900 uH
r_f	C_f	K_p	K_i	G_1	G_2
3 Ω	14 uF	2.9	1700	1	200

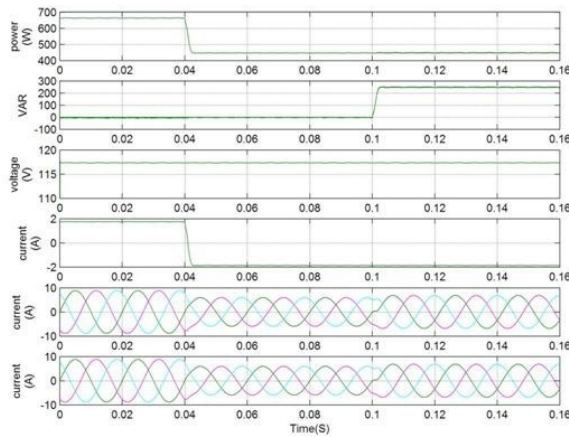


Fig. 12. Simulated results for the first scenario. (a) Active power injected to the grid. (b) Reactive power injected to the grid. (c) PV module DC voltage. (d) Battery current. (e) Inverter AC current. (f) Grid current

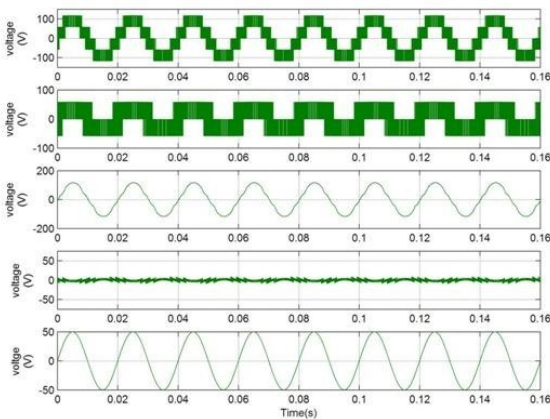


Fig. 13. Simulated inverter waveforms. (a) V_{ab} -Phase to phase inverter voltage. (b) V_{ao} -Inverter phase voltage reference to midpoint. (c) Filtered V_{on} -Filtered inverter phase voltage reference to midpoint. (d) Filtered V_{on} -Filtered midpoint voltage reference to neutral. (e) Filtered V_{an} -Filtered phase voltage reference toneutral

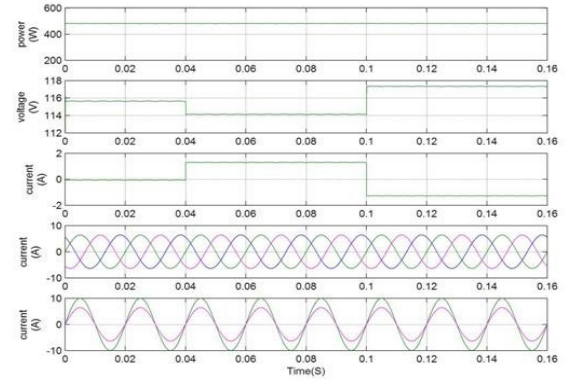


Fig. 14. Simulated results for the second scenario. (a) Active power injected to the grid. (b) PV module DC voltage. (c) Battery currents. (d) Grid side currents. (e) Grid side Phase (a) voltage and its current.

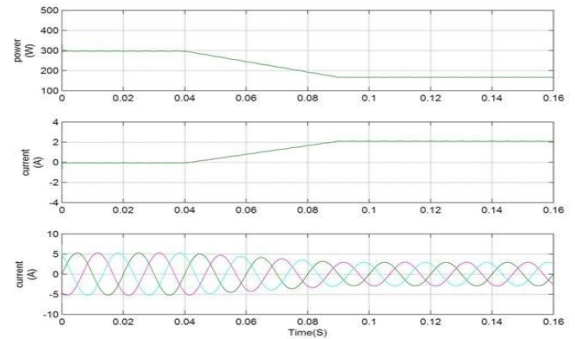


Fig. 15. Simulated results for third scenario. (a) Active power injected to the grid. (b) Battery current. (c) Grid side currents.

VI. CONCLUSION

A novel topology of both renewable energy and battery storage on the dc side of the inverter has been presented for a three-level NPC voltage source inverter will be integrated. A theoretical framework of a novel fuzzy logic control modulation technique will be used. That can generate the correct ac voltage under unbalanced dc voltage conditions has been proposed. For the proposed system has also been presented a new control algorithm in order to control power flow between solar PV, battery, and grid system, while MPPT operation for the solar PV is

achieved simultaneously. The effectiveness of the proposed fuzzy logic control topology and control algorithm was tested using simulations and results are presented. To control ac-side current, and battery charging and discharging currents at different levels of solar irradiation the results demonstrate that the proposed system is able.

REFERENCES

- [1] O. M. Toledo, D. O. Filho, and A. S. A. C. Diniz, "Distributed photovoltaic generation and energy storage systems: A review", *Renewable Sustainable Energy Rev.*, vol. 14, no. 1, pp. 506–511, 2010.
- [2] M. Bragard, N. Soltan, S. Thomas, and R. W. De Doncker, "The balance of renewable sources and user demands in grids: Power electronics for modular battery energy storage systems", *IEEE Trans. Power Electron.*, vol. 25, no. 12, pp. 3049–3056, Dec. 2010.
- [3] A. Yazdani and P. P. Dash, "A control methodology and characterization of dynamics for a photovoltaic (PV) system interfaced with a distribution network", *IEEE Trans. Power Del.*, vol. 24, no. 3, pp. 1538–1551, Jul. 2009.
- [4] A. Yazdani, A. R. Di Fazio, H. Ghoddami, M. Russo, M. Kazerani, J. Jatskevich, K. Strunz, S. Leva, and J. A. Martinez, "Modeling guidelines and a benchmark for power system simulation studies of three-phase single-stage photovoltaic systems", *IEEE Trans. Power Del.*, vol. 26, no. 2, pp. 1247–1264, Apr. 2011.
- [5] M. A. Abdullah, A. H. M. Yatim, C. W. Tan, and R. Saidur, "A review of maximum power point tracking algorithms for wind energy systems", *Renewable Sustainable Energy Rev.*, vol. 16, no. 5, pp. 3220–3227, Jun. 2012.
- [6] S. Burusteta, J. Pou, S. Ceballos, I. Marino, and J. A. Alzola, "Capacitor voltage balance limits in a multilevel-converter-based energy storage system", in *Proc. 14th Eur. Conf. Power Electron. Appl.*, Aug./Sep. 2011, pp. 1–9.
- [7] L. Xinchun, Shan Gao, J. Li, H. Lei, and Y. Kang, "A new control strategy to balance neutral-point voltage in three-level NPC inverter," in *Proc. IEEE 8th Int. Conf. Power Electron. ECCE Asia*, May/Jun. 2011, pp. 2593–2597.
- [8] J. Rodriguez, S. Bernet, P. K. Steimer, and I. E. Lizama, "A survey on neutral-point-clamped inverters," *IEEE Trans. Ind. Electron.*, vol. 57, no. 7, pp. 2219–2230, Jul. 2010.
- [9] A. Lewicki, Z. Krzeminski, and H. Abu-Rub, "Space-vector pulse width modulation for three-level npc converter with the neutral point voltage control", *IEEE Trans. Ind. Electron.*, vol. 58, no. 11, pp. 5076–5086, Nov. 2011.
- [10] J. Pou, D. Boroyevich, and R. Pindado, "Effects of imbalances and nonlinear loads on the voltage balance of a neutral-point-clamped inverter," *IEEE Trans. Power Electron.*, vol. 20, no. 1, pp. 123–131, Jan. 2005.
- [11] Z. Huibin, S. Jon Finney, A. Massoud, and B. W. Williams, "AnS